Int. J. Multiphase Flow Vol. 15, No. 4, pp. 531–552, 1989
Printed in Great Britain.

0301-9322/89 $3.00 + 0.00

PROCESSES WHICH CONTROL THE INTERFACIAL WAVE SPECTRUM IN SEPARATED GAS–LIQUID FLOWS

K. BRUNO† and M. J. MCCREADY
Department of Chemical Engineering, University of Notre Dame, Notre Dame, IN 46556, U.S.A.

(*Received* 12 *August* 1988; *in revised form* 31 *January* 1989)

Abstract—The behavior of the spectrum of short-wavelength waves that occur at the interface of separated, horizontal, gas–liquid flows is controlled by the rate at which energy is transferred from the gas flow into the liquid, the rate at which waves decay due to viscous dissipation and also by the nonlinear interactions between the various modes which cause an energy cascade through the spectrum. Measurements of evolving wave spectra, both with and without additional waves induced by an oscillating paddle, are used to examine energy input and interaction rates between waves. For cases where waves are induced, strong interactions between the induced wave and its first overtone, which increase as the layer gets thinner, are observed. An equation to describe steady wave spectra, which incorporates the effects of growth, dissipation and energy transfer in the form of interactions between a wave and its first overtone, is derived using a dynamic energy balance. The critical effects of layer depth, gas shear and surface geometry on the energy transfer rate are included in the analysis. The resulting spectral equation elucidates the important effects which control the wave composition of the gas–liquid interface and also provides reasonably good predictions of experimental wave spectra.

Key Words: interfacial waves, wave interactions, gas–liquid flows

1. INTRODUCTION

Waves occur at the interface of the separated flow regimes over a wide range of conditions. They are known to influence interfacial shear and thereby affect both the pressure drop and interfacial transport rates. In addition, qualitative changes in the wave patterns are of interest because they may signal impending flow regime transitions. Previous studies to identify the qualitative behavior of the interface (Hanratty & Engen 1957; Telles & Dukler 1970; Webb & Hewitt 1975) have noted that many different regimes exist and the behavior can be rather complex. However, it is convenient from a theoretical perspective to divide the waves into two primary types: waves with wavelengths much longer than the corresponding layer thickness (which may be either kinematic or dynamic in nature) and those with wavelengths on the order of or smaller than the layer thickness (which are dynamic waves in the capillary–gravity regime). The long waves have been linked to the transition to slug flow by Taitel & Dukler (1976) and Lin & Hanratty (1986) and have been shown to affect atomization by Woodmansee & Hanratty (1969). Back & McCready (1988a, b) demonstrated that it is possible to directly calculate interfacial mass transfer coefficients which accurately match experimental values without the use of any adjustable parameters from measured wave spectra of short waves. The surface roughness, which results from the presence of short-wavelength waves has been linked to the observed pressure drop by Andritsos & Hanratty (1987).

The present study will focus on conditions for horizontal stratified gas–liquid flows where short-wavelength waves are the dominant type. Waves will be described in terms of a surface deviation–frequency spectrum which is perhaps the simplest description that contains most of the quantitative information necessary to describe the wave field. A frequency spectrum for waves contains information about the average wave amplitude as a function of frequency. It is an appropriate instrument for use in the description of a random wave field which is comprised of numerous weakly interacting waves which are nearly sinuous in shape. Under these circumstances, the form of the spectrum is determined by both the rate at which energy is gained or dissipated by individual waves and by dynamic interactions between modes which lead to an energy flux through the spectrum. It is noted that the wave spectrum for waves with wavelengths much longer

†Present address: AMOCO Oil Co., Naperville, IL 60566, U.S.A.

than the layer thickness is distinctly different. Because long-wavelength waves will not interact very strongly and therefore not transfer energy to any significant extent, the shape of a spectrum of long waves will represent only the amplitudes of the various modes necessary to form the characteristic shapes of the waves.

Frequency spectra have been used to describe ocean and lake waves since the 1950s. The first theoretical predictions of the spectral shape which were done using dimensional analysis were suggested by Phillips (1958) for gravity waves and Hicks (1960) for capillary waves. Since this time, numerous theories (Hasselmann 1962, 1963; Valenzuela & Laing 1972; Phillips 1985) have been presented which attempt to include the ubiquitous nonlinear wave interactions that control the shape of the spectrum. However, due to the complexity of including all of the various wave interactions which occur in a wave field on a large body of water, only minimal success has been achieved at predicting the shape and magnitude of the wave spectrum. The present state of the art on this subject is given in the papers by van Gastel (1987) and Janssen (1987). These authors use direct numerical simulation of the wave field as it evolves in time. van Gastel considers only purely resonant interactions in all directions and Janssen considers collinear overtone interactions between two modes without imposing the condition that the speeds match. While these procedures appear promising and provide some quantitative and qualitative agreement with data, the complexity of the calculations and length of computing time necessary limit the utility of these approaches. In particular, it is time-consuming to use these methods to investigate the effects of various factors (e.g. interfacial stress, layer depth) on the spectrum.

Wave spectra in horizontal gas–liquid flows have been measured by Lilleleht & Hanratty (1961), Cohen (1964), Lleonart & Blackman (1980) and McCready & Hanratty (1985). The theoretical descriptions given by Lilleleht & Hanratty (1963) and Lleonart & Blackman (1980) were based on dimensional analysis. While some agreement between experiments and theory occurs, dimensional analysis is not an entirely satisfactory method for describing the wave spectrum because the dynamical nature of the problem, the importance of wave–wave interactions, is missed. McCready (1986) showed that it was possible to include wave interactions through the use of a dynamic balance for the wave energy. Using a procedure similar to that of Pao (1965) for turbulence, he showed if energy transfer occurred by overtone interactions, the shape of the capillary region of the spectrum ($f > 40$ Hz) was accurately described. However, as no energy input was included in his equation, it was not possible to predict the region around the peak which corresponds to the largest waves present and is of greatest practical interest.

In this paper, the individual processes which control the shape of the spectrum, energy input and energy transfer by nonlinear interactions, are examined experimentally and theoretically. A dynamic energy balance, which includes energy input as well as dissipation and energy transfer by nonlinear interactions, is developed for the wave spectrum. Energy input and dissipation are described by using predictions of linear stability analysis. Nonlinear energy transfer, including the effects of layer depth and interfacial shear, is described as occurring through the interaction of a fundamental wave with its first overtone. Calculations using this theory demonstrate how various parameters influence the spectrum. Quantitative predictions of the spectrum are compared to measurements for numerous flow conditions and several liquid viscosities. In general, good agreement occurs.

2. EXPERIMENT

A detailed discussion of the experimental apparatus and technique used to measure the wave spectra and wave properties is given by Bruno & McCready (1988). The flow system in which the concurrent gas–liquid flows were studied consists of a horizontal, rectangular channel which has a flow area 2.54 cm high, 30.5 cm wide and a total length of about 8.5 m. Air is introduced into one end of the channel through a converging entrance section. Liquids, which consist of either water or a glycerin–water mixture, enter the channel through slots in the bottom of the channel about 10 cm downstream from the gas entrance. A wire mesh screen covers the liquid entrance to minimize disturbances. The gas and liquid exit the channel into a large separating drum which allows for recycle of the liquid and prevents any reflection of waves upstream. Experiments presented here cover a wide range of gas and liquid flow rates but specifically exclude conditions where roll waves are present.

Interfacial and wall shear stresses were determined from the pressure drop measurements using a micromanometer and the location of the zero stress plane obtained by traversing a Pitot tube between the gas–liquid interface and the top of the channel. Interfacial velocities were determined by placing thin computer card punched rectangles onto the gas–liquid interface and timing their progression over a known distance. Wave surface tracings were acquired by using a parallel-wire conductance technique that has been described previously by Miya *et al.* (1971) and McCready (1986). The wires are 0.0127 cm dia and are spaced 0.3 cm apart. Data are presented in the form of either surface tracings or wave spectra which are Fourier-transforms of the surface tracing time series. The spectral function $\phi(f)$ is defined as

$$\overline{a^2} = \int_0^\infty \phi(f)\,\mathrm{d}f, \qquad [1]$$

where $\overline{a^2}$ is the variance of the instantaneous surface displacement and f is frequency. In this paper, the frequency spectrum is calculated from the surface time series using the IMSL subroutine FTFPS. To test its suitability for accurately resolving narrow peaks, we have calculated the spectra of various analytical functions and have found no evidence of spurious peaks.

3. PROCESSES ASSOCIATED WITH THE WAVE SPECTRUM

The shape of steady wave spectra observed in gas–liquid flows is determined by the combined effect of the energy input from the gas flow, viscous dissipation and nonlinear wave interactions which allow transfer of energy between different wave modes. To describe the shape of the wave spectrum, it is necessary to characterize all of these processes and use them in a governing equation.

(*a*) *Wave interactions*

It is known from the work of McGoldrick (1965), that finite amplitude capillary–gravity waves will engage in energy transfer among members of triads which satisfy the resonance conditions. Kim & Hanratty (1971) showed that equally important, similar, three-mode interactions occur between collinear waves which belong to a family of harmonics. A wave field generated by a turbulent gas flow will contain a broad distribution of harmonics which will lead to numerous possible wave interactions. The shape of the wave spectrum is strongly determined by the net effect of these interactions. van Gastel (1987) estimates, considering only resonant interactions, that nonlinear interactions dominate the linear growth and decay processes in controlling the shape of the spectrum.

When formulating the effect that nonliear interactions will have in determining the shape of the spectrum, the primary questions which arise are: which interactions are dominant and how to account for them. van Gastel (1987) and Janssen (1987) have attempted to include all possible mode interactions (subject to specific assumptions) in their calculations of the spectrum. However, this leads to unnecessary complexity as many of the interactions are merely incidental to the determination of the shape of the spectrum. As demonstrated by the theory of Kim & Hanratty (1971), interactions between all of the waves in an overtone series are expected to be occurring in a spectrum of waves generated by gas shear. Because interaction rates are strongly dependent on the amplitude of the participating waves, the dominant interactions will be between the fundamental mode (which are the waves which comprise the peak of the specturm and therefore have the largest amplitudes) and the mode which has the largest amplitude of all the overtones. Since the spectra decay smoothly as the frequency increases, the overtone with the largest amplitude is always the first one.

Experiments to track the development of the wave field when waves are induced artificially with an oscillating paddle were done. Not unexpectedly, strong interactions were observed between a fundamental wave and its first overtone and in some cases, higher overtones as well. This frequency-doubling interaction was clearly observed for paddle-induced waves between 5 and 15 Hz. It should be noted that these interactions do not satisfy the resonance criteria.

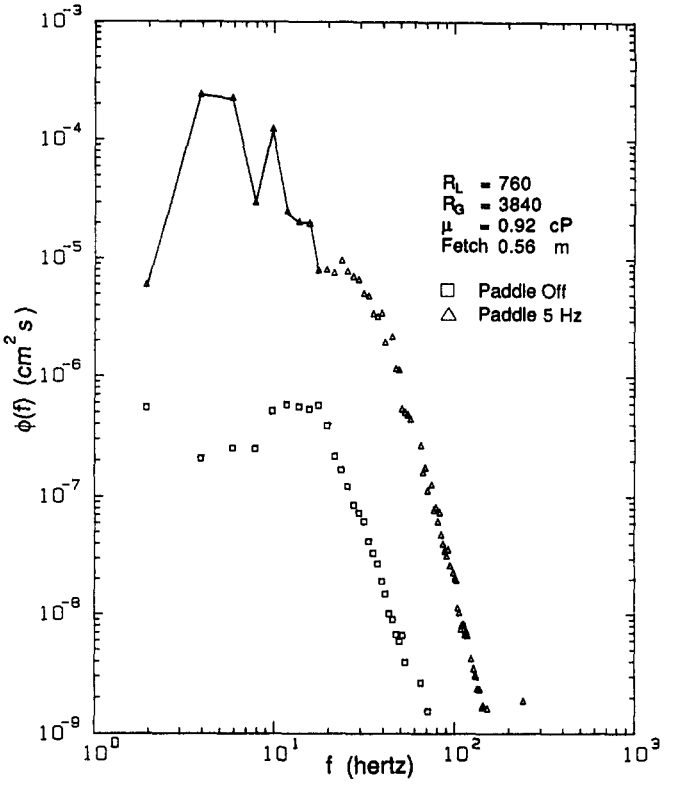

Figure 1. Wave spectra depicting the effect of paddle-induced waves and the interactions which result. $\bar{h} = 0.47$ cm, $v^* = 0.63$ cm/s.

One example of the frequency-doubling interaction is seen in figure 1. In this figure, when the paddle is off, the spectrum has a relatively flat peak between 10–20 Hz as these waves have about the same amplitude. However when the paddle is operated at 5 Hz, a strong overtone interaction is seen between the 5 and 10 Hz waves; spectral waves before and after 10 Hz are almost one order of magnitude smaller, suggesting a direct 5–10 Hz interaction. The surface tracing, shown in figure 2a, for the case where the paddle is operating shows the dominant 5 Hz wave. The 10 Hz mode and some higher overtones are also present, as evidenced by the additional bumps which occur on the 5 Hz oscillations.

The effect of layer depth on the interaction is demonstrated by comparing figures 1 and 3, where the layer thickness has been decreased from 0.47 to 0.31 cm. In figure 3, large spectral magnitudes are seen at about 5, 10, 15 and 20 Hz. For these conditions, energy transfer from the fundamental to its overtones is so rapid that more energy is found in the overtones than the fundamental. This spectrum is consistent with the results of Kim & Hanratty (1971) who showed theoretically and experimentally that the effect of decreasing the layer depth is to increase the interaction rate between all harmonics and allow for more waves in the overtone series to be excited more rapidly. In figure 2b, the surface tracing which corresponds to figure 3 clearly shows presence of four distinct modes.

A final example of a fundamental–first overtone interaction is provided in figure 4, where the paddle is operated at 15 Hz and produces 30 Hz overtones. The types of wave interactions occurring when the paddle was operated at frequencies higher than about 15 Hz were not clearly detectable in a wave spectrum because these waves interacted quickly and became an indistinguishable part of the random wind-generated wave field.

(*b*) *Wave growth and dissipation*

Another process controlling the composition of the interface is the net growth rate, which is the difference between the energy input rate to waves and the wave energy dissipation rate. The frequency range of the unstable, hence growing, waves shifts with each set of flow conditions and

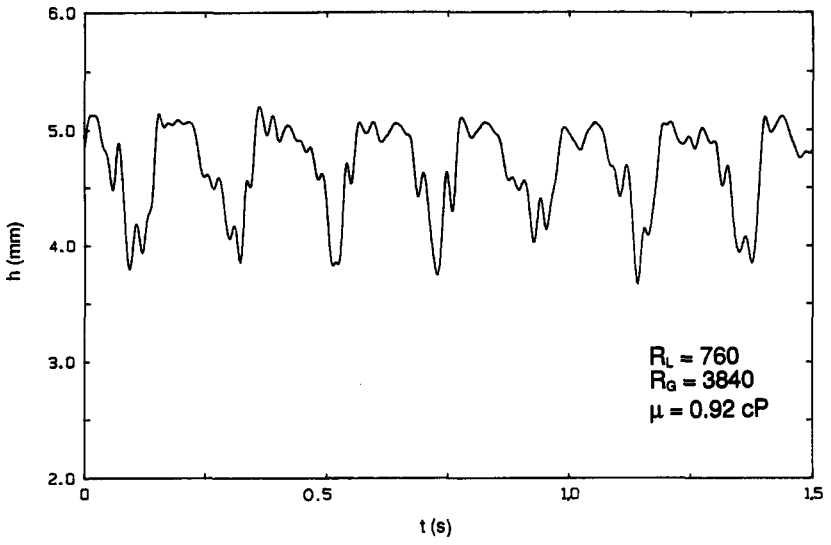

Figure 2a. Surface tracing of 1.5 s in duration for the conditions of figure 1. Disturbances of higher frequencies are present along with the dominant 5 Hz wave.

can be calculated from linear stability analysis (Hanratty 1983). Since the nature of the interface is a strong function of a selective net growth process, the wave spectrum, being a quantitative measure of the interface, is also dependent on the net growth rate. The basic phenomena of wave growth, dissipation and energy transfer are interrelated in a wave field and spectrum because wave interactions transfer energy from the most unstable waves to higher frequency waves capable of rapidly extinguishing the wave energy through viscous dissipation. These basic processes define the dynamic energy balance.

In the spectral equation developed in section 4, the net growth rate will be calculated from the Orr-Sommerfeld linear stability analysis performed by Cohen & Hanratty (1965). While linear stability theory can only approximate the energy input which occurs for finite amplitude waves, it is expected to give reasonable answers because wave slopes are typically < 0.1. In the stability

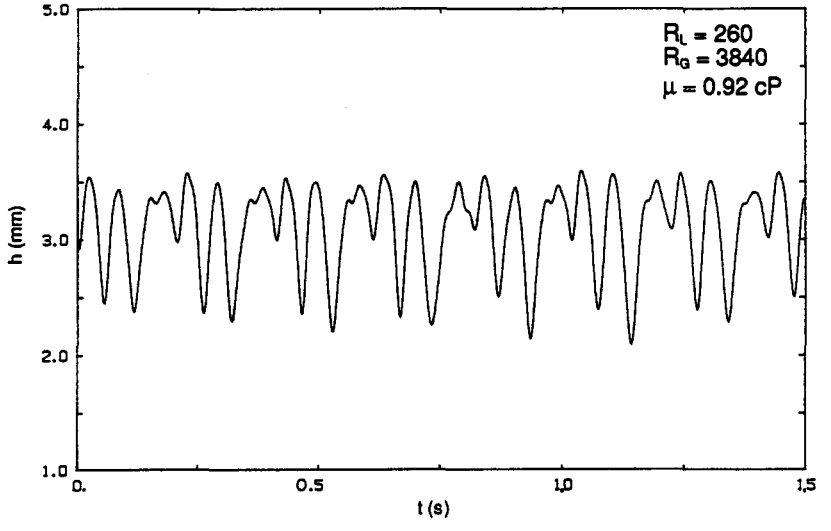

Figure 2b. Surface tracing of 1.5 s in duration for a layer which is thinner than in figure 2b. Because of nonlinear interactions, the original 5 Hz wave has evolved into an overtone series with the 15 Hz wave being the dominant mode. $\bar{h} = 0.305$ cm, $v^* = 0.52$ cm/s.

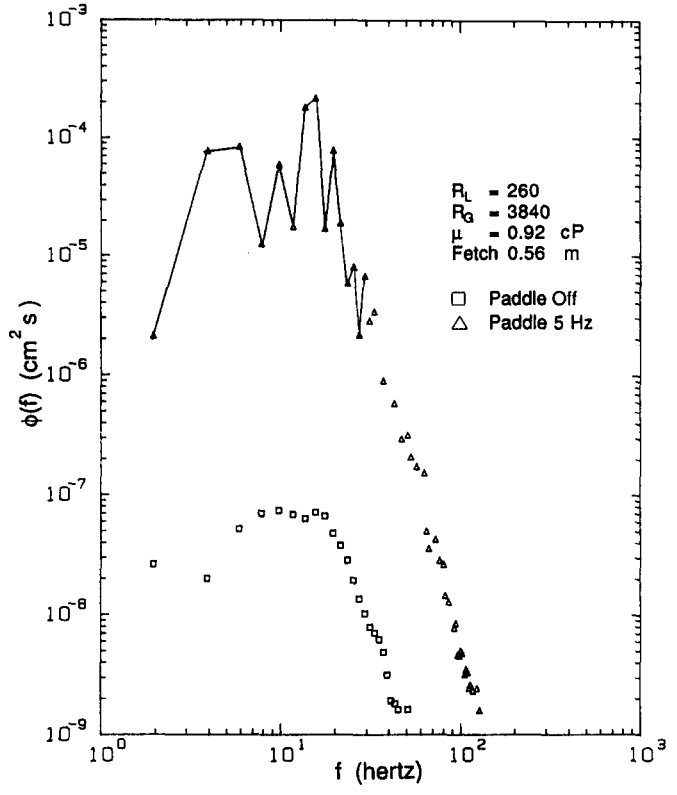

Figure 3. Wave spectra for the conditions of figure 2b. Interactions occur at a faster rate as the layer thickness decreases. This allows for greater transfer of energy to overtones in the same distance.

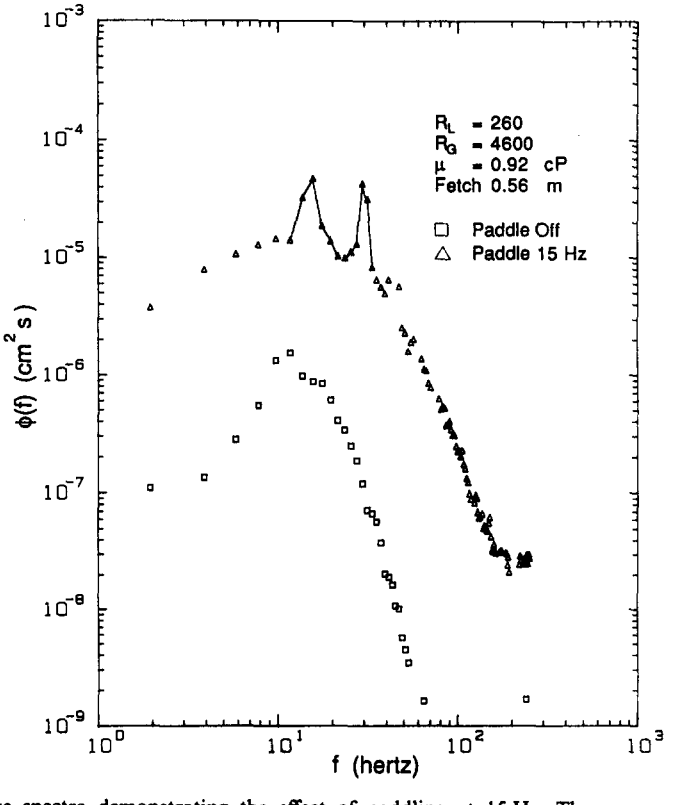

Figure 4. Wave spectra demonstrating the effect of paddling at 15 Hz. The more common case of generation of a single overtone is depicted. $\bar{h} = 0.31$ cm, $v^* = 0.61$ cm/s.

analysis, the wave speed (eigenvalue) c is complex with the real part c_R giving the wave speed; waves are predicted to grow for positive values of the imaginary part c_I which determines stability. Cohen & Hanratty solved the Orr-Sommerfeld equation for the liquid phase using the boundary conditions that the normal and tangential velocity components vanish at the bottom wall and by balancing the normal and shear stresses across the gas–liquid interface. A linear velocity profile is also employed. The corresponding growth factor αc_I is proportional to the net growth rate and is given by

$$\alpha c_I = \frac{\left\{\frac{\hat{P}_{sI}}{\rho_L} + \frac{\hat{\tau}_{sR}}{\rho_L \alpha}\left[\alpha \coth(\alpha\bar{h}) + \frac{v^{*2}}{\nu_L(c_R - U_0)}\right] - 4\alpha^2\nu_L(c_R - U_0)\coth(\alpha\bar{h}) - 4\alpha v^{*2} - \frac{\alpha^{\frac{3}{2}}\nu_L^{1/2}(\coth^2\alpha\bar{h} - 1)c_R^{1/2}(c_R - U_0)^2}{(2)^{1/2}c_R}\right\}}{\left[2(c_R - U_0)\coth(\alpha\bar{h})\frac{v^{*2}}{\nu_L\alpha}\right]}. \quad [2]$$

The wavenumber is denoted by α, ρ_L and ν_L are the liquid density and kinematic viscosity respectively, U_0 and v^* are the liquid interfacial and friction velocities and $\bar{h}$ is the average layer thickness. The pressure and stress variations are represented as a single sinuous function given by the parameters $\hat{\tau}_s$ and $\hat{P}_s$, where the subscript I refers to the component in phase with the wave slope and R denotes the component in phase with the wave height. In [2], the first two terms on the r.h.s. are positive and therefore promote growth through pressure fluctuations ($\hat{P}_{sI}$) in phase with the wave slope and shear stress ($\bar{\tau}_{sR}$) fluctuations in phase with the wave height. The last three terms are negative, with terms three and four representing internal viscous dissipation (prevalent at high velocities) and the fifth term being a measure of bottom wall dissipation, which becomes relatively more important as the wavelength-to-layer depth ratio increases.

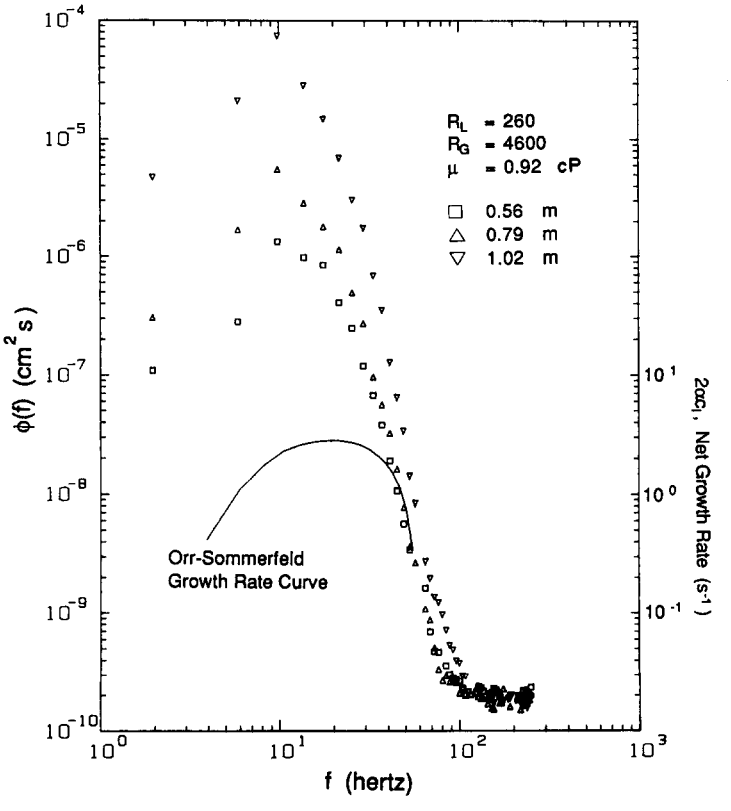

Figure 5. Initial growth of the wave spectrum as a function of fetch compared with linear growth rates of predicted by an Orr-Sommerfeld equation. $\bar{h} = 0.38$ cm, $v^* = 0.61$ cm/s.

Wave spectra were measured at increasing fetch (distance from initial gas–liquid contact point) to depict initial wave growth and one example is presented in figure 5. Also included in this figure is the growth rate curve calculated from [2]. The caret quantities in αc_1 were estimated using Abrams' (1984) data for the flow of a turbulent liquid over a solid wavy surface. Bruno (1988) has shown that these quantities should be applicable to gas–liquid systems because the gas–viscosity ratio is sufficiently small (0.02–0.01) and the wave speeds are much slower than the maximum gas velocity (leading to no singularity in the Orr-Sommerfeld equation). The shape and location of the theoretical growth rate curve are consistent with the spectra; the most unstable Orr-Sommerfeld waves generally correspond to the fastest growing peak spectral waves and the magnitude of the spectra falls off dramatically on both sides of the peak in agreement with linear stability analysis. In addition, the experimental spectra suggest that the initial growth rate is exponential since the peak amplitudes increase exponentially with distance. This observation is consistent with the stability analysis assumption of exponential growth and also in agreement with the single wave growth experiments of Larson & Wright (1975).

4. THEORETICAL DEVELOPMENT OF THE SPECTRAL EQUATION

The motivation to derive an equation to predict the spectrum is first, to demonstrate the effects of flow parameters such as the friction velocity and layer height on the nature of the interface, thus leading to a better understanding of the controlling processes. Secondly, the spectral equation derived here provides a reasonably accurate approach for quantitatively predicting the characteristics of the gas–liquid interface. This development utilizes linear wave speeds, weakly nonlinear interactions and net growth rates calculated from the Orr-Sommerfeld analysis. While the interactions are probably correctly explained by the weakly nonlinear approach, actual waves may travel at speeds and experience growth rates different from the linear predictions. In addition, the inherent three-dimensionality of the problem is important and cannot be explicitly included. Therefore, this development should not be viewed as a rigorously correct attempt to predict the spectrum for idealized conditions [such as van Gastel (1987) or Janssen (1978)] but, rather, as a study to discover why wave spectra behave as they do in gas–liquid flows.

(*a*) *Spectral energy balance*

The premise underlying this deviation is that a continuous cascade of energy from low to high frequencies occurs. Energy is fed into primarily the fastest growing inertial waves ($\sim$10–30 Hz) which provide an energy source for all other waves. The majority of energy is transferred upward

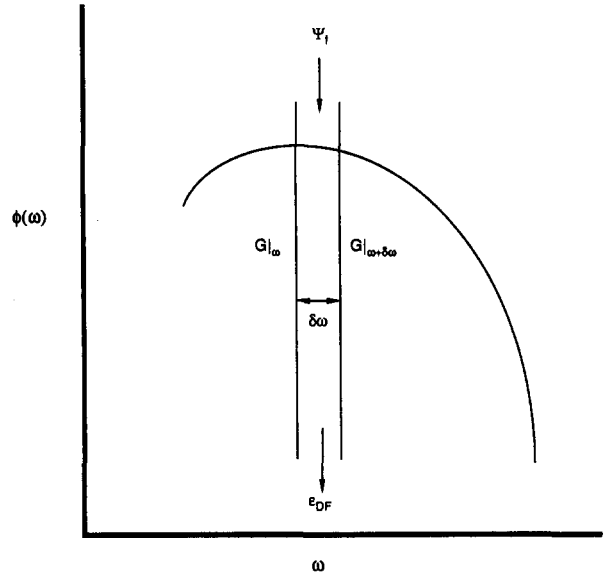

Figure 6. Diagram of the processes which govern the wave spectrum.

in frequency to shorter-wavelength waves which in turn quickly dissipate it at a rate proportional to the square of their amplitude. In this development, only transfer upward in frequency between a wave and its first overtone is considered.

Consider an energy balance around the spectral element $\delta\omega(\omega = 2\pi f)$, given in figure 6. Three competing phenomena are simultaneously occurring—each to a different degree depending upon the frequency interval of interest. First, the flux of energy (energy/$\delta\omega$/time) from the gas to the liquid phase which promotes wave growth is defined as ψ_F. Secondly, irreversibly lost in each spectral element is a wave dissipation energy flux, denoted by ϵ_{DF}. This energy loss is composed of internal viscous and bottom wall dissipative effects. The third component of the energy balance is attributed to the net energy transfer rate G (either upward or downward in frequency) resulting from nonlinear wave interactions. Energy enters the spectral element from lower frequencies at a net rate defined by $G|_\omega$ and is transferred out of the element at a rate given by $G|_{\omega+\delta\omega}$. The governing energy balance over each spectral element is therefore

$$G|_\omega + \psi_F \delta\omega = G|_{\omega+\delta\omega} + \epsilon_{DF}\delta\omega. \quad [3]$$

Taking the limit as $\delta\omega \to 0$ yields the differential equation

$$\frac{dG}{d\omega} = \psi_F - \epsilon_{DF}, \quad [4]$$

which, after substituting expressions for G, ψ_F and ϵ_{DF} in terms of $\phi(\omega)$, will provide the spectral equation.

(b) Energy transfer

There are at least two similar ways of addressing the question of the rate at which energy transfer occurs. McCready (1986) followed the ideas of Heisenberg (1948) and Pao (1965) for homogeneous turbulence and assumed that the net rate of energy transfer is the product of the total energy per element $\delta\omega$ over which [4] is numerically integrated and the rate of transfer of that element to other frequencies. The total wave kinetic and potential energy per element $\delta\omega$ is

$$E_{\delta\omega} = E_0\phi(\omega), \quad [5]$$

where

$$E_0 = \frac{1}{4}\left[\rho_L g + \sigma\alpha^2 + \rho_L \frac{\omega^2}{\alpha}\coth(\alpha\bar{h})\right], \quad [6]$$

with σ denoting interfacial tension divided by liquid density. The rate of transfer of energy in that element is given the symbol F and hypothesized to be

$$F = \frac{\Delta\omega}{\tau_I}, \quad [7]$$

where $\Delta\omega$ is the frequency difference between the interacting waves and τ_I is the characteristic time constant of the interaction. Therefore the intermediate form of G is

$$G = E_0\phi(\omega)\frac{\Delta\omega}{\tau_I}. \quad [8]$$

If most of the net energy transfer occurs by the overtone interactions between a fundamental and its first overtone, then the change in frequency, $\Delta\omega$, will be equal to ω_1, the frequency of the fundamental. Therefore, by definition, $\Delta\omega$ reduces to

$$\Delta\omega \approx 2\omega_1 - \omega_1 = \omega. \quad [9]$$

Admittedly all interactions do not behave according to [9]. However, Kim & Hanratty (1971) have shown that before a higher harmonic can be excited, all lower harmonics must be present.

The characteristic time constant τ_I is a measure of how quickly the interaction occur. For waves on an infinitely deep layer without gas shear, McGoldrick (1965) shows that the functional form of τ_I is

$$\tau_I \sim \frac{1}{\omega\alpha a}, \qquad [10]$$

for regular two-dimensional waves. For the present wave field which consists of a distribution of wave modes and varying degrees of three-dimensionality (depending upon flow conditions and physical properties), the relation is more complex and the proportionality constant cannot be determined theoretically. As a consequence, it is necessary to include an empirical geometric factor which accounts for the randomness and degree of three-dimensionality of the surface. Experimental observations indicate that as the liquid viscosity is increased, the waves become more two-dimensional. The degree of randomness is also affected by viscosity as well as flow conditions. In this analysis, these effects will be lumped together into a coefficient Q by using a relation of the form

$$Q = K\frac{\mu_L}{\mu_W}, \qquad [11]$$

where μ_L and μ_W are the dynamic viscosities of the liquid and water, respectively. The form of [11] and the value of K, an $O(1)$ proportionality constant, were determined by fitting experimental spectral data. It is noted that the present Q differs from that used by McCready (1986) by the inclusion of the viscosity ratio. In terms of the spectral function, the interaction time becomes

$$\tau_I = \frac{1}{Q\omega\alpha[\phi(\omega)]^{1/2}(\delta\omega_D)^{1/2}}, \qquad [12]$$

where $\delta\omega_D$ is the discretization interval for the numerically generated spectrum. The question which arises is, should the time scale be determined by the properties of the overtone or the fundamental? To determine this, we calculated τ_I at each point along the spectrum and found that the two time scales were of the same order but that the slower time scale, and presumably the one which determines the rate of interaction, was always the lower frequency wave. Thus, the rate of energy transfer for random waves where there is no gas shear may be obtained by combining [7], [9] and [12] and evaluating the variables at the value of the lower frequency wave. No knowledge of the magnitude of the spectrum at the frequency of the overtone is needed and as a result, it is possible to calculate the spectrum by integrating a differential equation upward in frequency without any iteration being necessary.

This derivation, which relies basically on dimensional arguments is a simplification of the actual situation. A second method of addressing the rate of energy transfer between regular two-dimensional, traveling waves with no gas shear, has been determined explicitly by Kim & Hanratty (1971) (their equation [14]). Translating their notation into ours, we find that the functional form is the same as above but that τ_I should be evaluated at the frequency of the overtone. As mentioned above, both of the time scales (τ_I) were of the same order and change in the same fashion, so the time scale calculated from the fundamental frequency was used in this work because it obviates the need for iteration in the solution. In addition, the value of the spectral function is always known more accurately at lower rather than at higher frequencies (because of the initial value nature of the problem), so it was felt that more consistent results would occur if the time scale of the lower frequency was used.

(c) *Effects of gas shear and liquid depth*

Kim & Hanratty (1971) discovered that the wave interaction rate increases for decreasing layer depth. An explanation for this behavior is that as the layer becomes thinner, the waves become less dispersive and their celerities all approach twice the average liquid velocity. It is much easier for waves traveling at nearly the same speed to interact, therefore the interaction rate increases (τ_I decreases). Interaction coefficients arise in Kim & Hanratty's amplitude equation and each coefficient corresponds to a different type of interaction. These interaction coefficients are measures of how the layer depth affects a given interaction rate. The interaction coefficient in their work

which is relevant to this development is P_4, which provides the effect of layer depth on the transfer of energy from a wave to its first overtone:

$$P_4 = \frac{1}{8[2k]}([k]^2 + 4[k][2k] - 3) \quad [13a]$$

and

$$[nk] = \coth(n\alpha\bar{h}). \quad [13b]$$

In a similar manner, Janssen (1986) derives an amplitude equation for an infinitely deep layer that includes the shearing effect of the gas phase. An increase in the shear rate increases the interaction coefficients and hence the rate of interactions because the orbital motions associated with traveling waves are forced to become more asymmetric (stretching occurs in the flow direction) due to the liquid velocity gradient and can therefore interact over a larger distance. The dimensionless coefficient for upward energy transfer for a fundamental–first overtone interaction which accounts for shear is

$$\beta = \frac{\alpha\bar{h}^2 \dfrac{(c_R - U_0)G_0}{U_0}}{2\left(1 - \dfrac{\mu_0}{4}\right)}, \quad [14a]$$

where

$$G_0 = 1 - 2\mu_0 + 2\mu_0^2 \quad [14b]$$

and

$$\mu_0 = \frac{v^{*2}}{v_L\alpha(U_0 - c_R)}. \quad [14c]$$

As the interaction rate is proportional to P_4 and β, the increase in the magnitude of P_4 with decreasing depth and β with increasing gas shear (or friction velocity) are consistent with the experiments shown above. To properly apply P_4 and β to τ_1, the resulting functional representation of the characteristic time constant is

$$\tau_1 = \frac{1}{QP_4\beta\omega\alpha[\phi(\omega)]^{1/2}(\delta\omega_D)^{1/2}}. \quad [15]$$

At this point the energy transfer function G is completely defined and equal to

$$G = QP_4\beta\omega^2\alpha E_0[\phi(\omega)]^{3/2}(\delta\omega_D)^{1/2}. \quad [16]$$

(d) Net growth rate

The next task is to determine $\psi_F - \epsilon_{DF}$. The change in total wave energy E_T with respect to time in the absence of wave interactions is equal to the difference between the rate of energy input from the wind and wave dissipation:

$$\frac{dE_T}{dt} = (\psi_F - \epsilon_{DF})\delta\omega_D. \quad [17]$$

The energy of a wave is proportional to the wave amplitude a and takes the following form from linear stability analysis:

$$a = a_0 \exp\{i\alpha[x - (c_R + ic_I)t]\}. \quad [18]$$

From [18] it is seen that when c_I is positive, the wave amplitude grows (is unstable) and, conversely, when c_I is negative the wave remains stable and hence does not grow. Starting with the definition of the total energy in terms of the wave amplitude,

$$E_T = E_0 a^2, \quad [19]$$

and then taking dE_T/dt and collecting only the real parts, one obtains

$$\frac{dE_T}{dt} = E_0 2(\alpha c_1) a^2, \tag{20a}$$

where the net growth rate is seen to be proportional to αc_1. In spectral notation, [20a] is

$$\frac{dE_T}{dt} = E_0 2(\alpha c_1)\phi(\omega)\delta\omega_D. \tag{20b}$$

Substituting [20b] into [17] provides the desired result of

$$\psi_F - \epsilon_{DF} = 2E_0(\alpha c_1)\phi(\omega). \tag{21}$$

The only unknown quantity in [21] is αc_1, which is calculated from [2]. The dispersion relation given by Cohen & Hanratty (1965), which accounts for Doppler shifting and the effect of the friction velocity,

$$c_R = U_0 - \frac{v^{*2}}{2\nu_L\alpha}\tanh(\alpha\bar{h}) + \left[\left(\frac{v^{*2}}{2\nu_L\alpha}\tanh(\alpha\bar{h})\right)^2 \tanh(\alpha\bar{h})\left(\frac{\alpha\sigma}{\rho_L} + \frac{g}{\alpha} + \frac{\hat{P}_{sR}}{\rho_L\alpha}\right)\right]^{1/2}, \tag{22}$$

is used to relate α, ω and c_R in all the appropriate equations.

Substituting [2] into [21] and [16] into [4] yields the final form of the nonlinear spectral equation:

$$\frac{d\{QP_4\beta\omega^2\alpha E_0[\phi(\omega)]^{3/2}(\delta\omega_D)^{1/2}\}}{d\omega} = 2\alpha c_1 E_0\phi(\omega). \tag{23}$$

This equation is solved numerically. The solution method, values of the constants and a comparison between the numerical and experimental results are presented in the next section.

5. THEORETICAL AND EXPERIMENTAL RESULTS

Equation [23] is solved numerically using the trapezoidal rule. Experimental spectra indicate that under most conditions, the energy drops to zero at low frequencies. Consequently, the initial condition used in [23] for all solutions presented in this section is $\phi(2\pi) = 1 \times 10^{-9}$, corresponding to an initial frequency of 1 Hz. The solution was insensitive to changes in the magnitude of $\phi(2\pi)$, as long as it was kept $\lesssim 10^{-6}$.

The integration interval used to solve [23] was a $\delta\omega_D$ value of $0.2(2\pi)$. Smaller intervals produced nearly identical results and this was chosen as the optimum frequency spacing. For this value of $\delta\omega_D$, the proportionality constant $K = 0.61$. This value for K was selected to produce the best match between the theoretical and experimental spectra at an average set of flow conditions for both water and a 2.5 cP glycerin–water solution. The same value is used for all cases shown in this paper; there are no further adjustments in its value. It is noted that interaction times calculated from [15] using this value of K and the assumed functional form of [11] agree well with the times reported by van Gastel (1987). This agreement supports both the form of [11] and the value of K.

A comparison between the experimental and corresponding theoretical spectra calculated [23] is given in figures 7–16. In figures 7–11 the liquid is water with a viscosity of 0.92 cP, in figures 12–15 the liquid is glycerin–water mixture with a viscosity of 2.5 cP and in figure 16 the liquid is a glycerin–water mixture with a viscosity of 3.5 cP. In each figure the experimental spectral data are denoted by symbols. The experimental spectra were measured at a fetch of 6.0 m. By this distance, the wave fields have become uniform as the frequency spectra are nearly identical for fetch values > 3–4 m. The solid curves in figures 7–16 are the theoretical spectra calculated from [23] and the dispersion relation [22] is used to iteratively calculate the wavenumber α at each frequency.

It is of interest to first examine the data. The total area under the wave spectral curves is observed to increase with increases in both friction velocity and liquid depth. If spectra at approximately the same v^* and $\bar{h}$, but different viscosities (e.g. cf. spectra 7c to 12a, 8b to 16a or 10c to 14a) are compared, the lower viscosity fluid generally has a higher peak (although spectrum 7c to 12a is a counter example). There is a substantial difference which is observed in the shape of these comparable spectra if the peaks are superimposed. The spectrum for the more viscous fluid decays

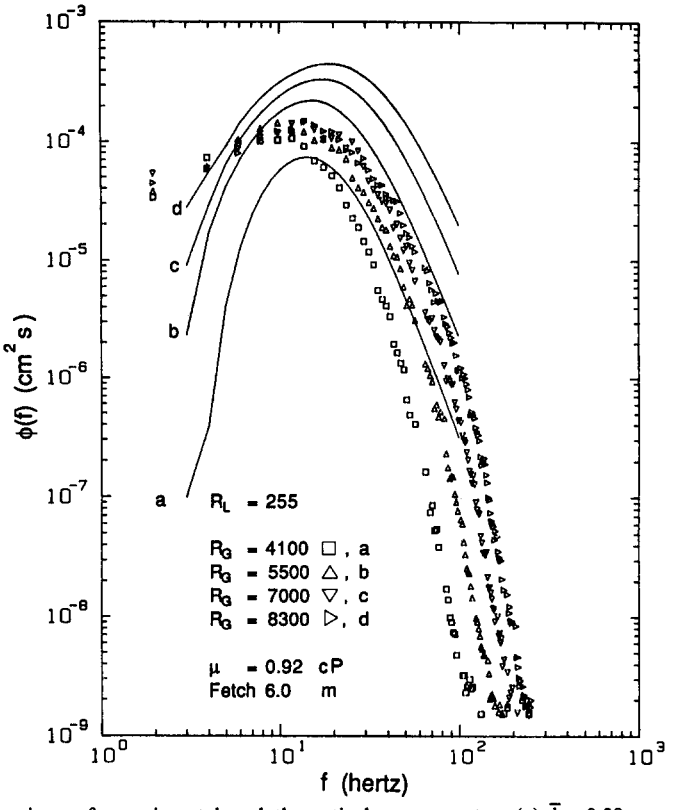

Figure 7. Comparison of experimental and theoretical wave spectra. (a) $\bar{h} = 0.38$ cm, $v^* = 0.55$ cm/s; (b) $\bar{h} = 0.37$ cm, $v^* = 0.73$ cm/s; (c) $\bar{h} = 0.35$ cm, $v^* = 0.88$ cm/s; (d) $\bar{h} = 0.32$ cm, $v^* = 1.04$ cm/s.

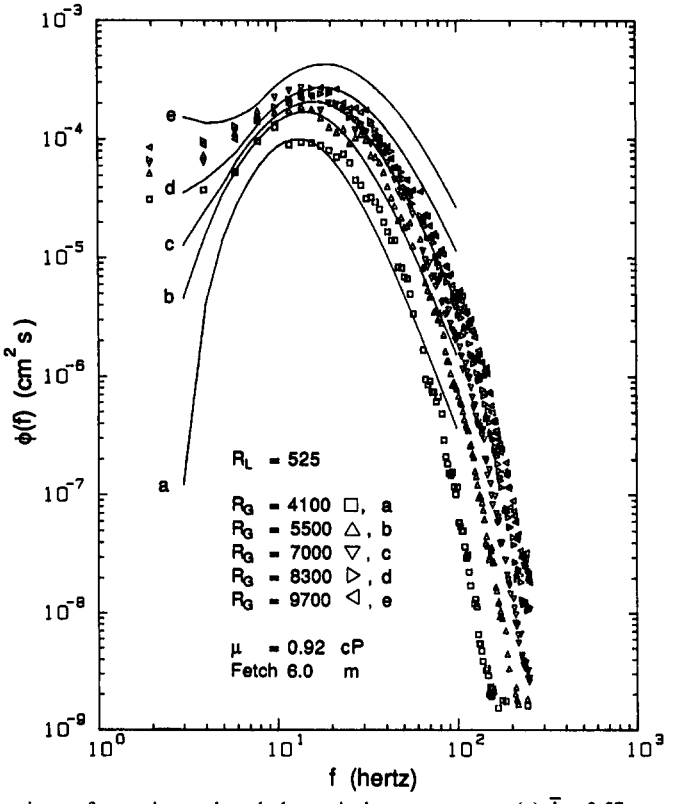

Figure 8. Comparison of experimental and theoretical wave spectra. (a) $\bar{h} = 0.57$ cm, $v^* = 0.59$ cm/s; (b) $\bar{h} = 0.55$ cm, $v^* = 0.78$ cm/s; (c) $\bar{h} = 0.53$ cm, $v^* = 0.95$ cm/s; (d) $\bar{h} = 0.48$ cm, $v^* = 1.12$ cm/s; (e) $\bar{h} = 0.43$ cm, $v^* = 1.29$ cm/s.

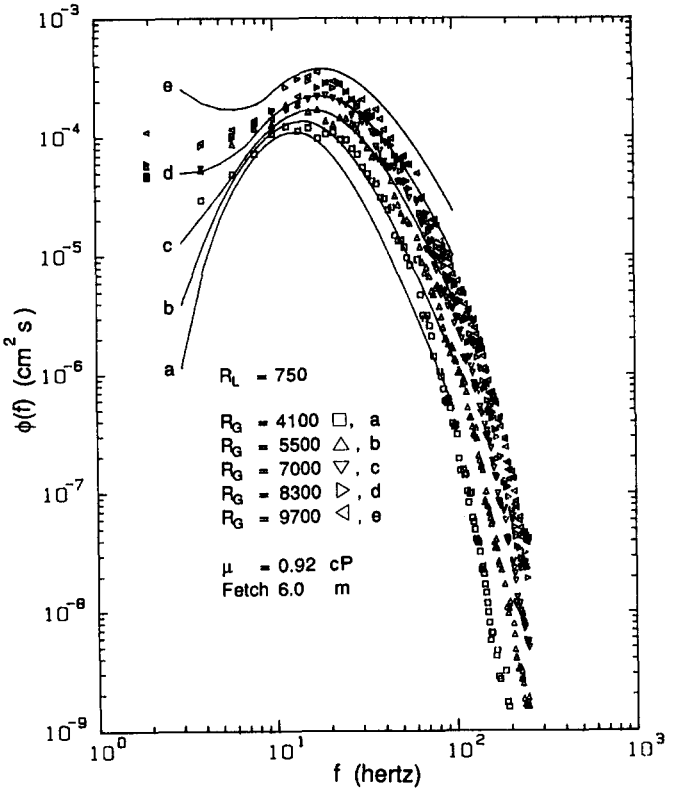

Figure 9. Comparison of experimental and theoretical wave spectra. (a) $\bar{h} = 0.68$ cm, $v^* = 0.65$ cm/s; (b) $\bar{h} = 0.67$ cm, $v^* = 0.78$ cm/s; (c) $\bar{h} = 0.61$ cm, $v^* = 0.97$ cm/s; (d) $\bar{h} = 0.56$ cm, $v^* = 1.15$ cm/s; (e) $\bar{h} = 0.50$ cm, $v^* = 1.33$ cm/s.

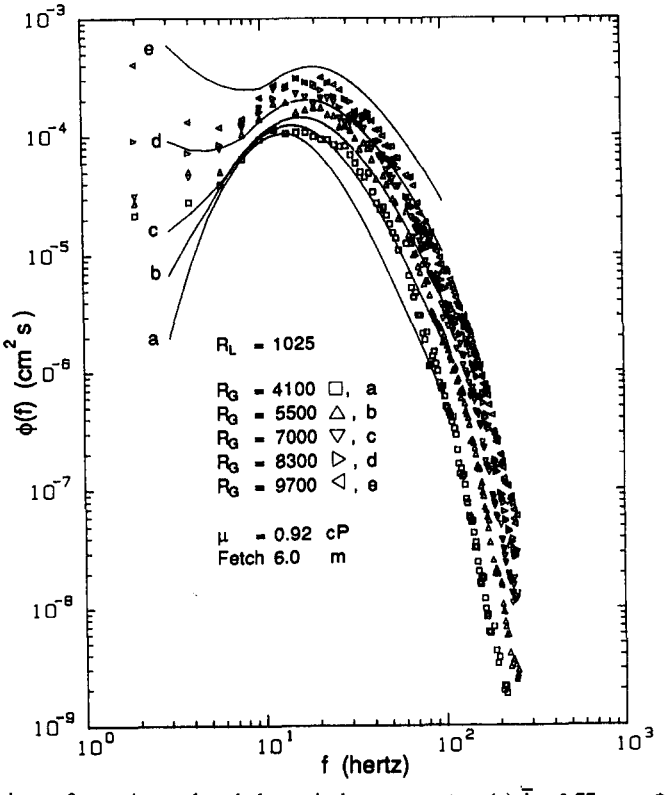

Figure 10. Comparison of experimental and theoretical wave spectra. (a) $\bar{h} = 0.77$ cm, $v^* = 0.69$ cm/s; (b) $\bar{h} = 0.73$ cm, $v^* = 0.86$ cm/s; (c) $\bar{h} = 0.68$ cm, $v^* = 1.00$ cm/s; (d) $\bar{h} = 0.62$ cm, $v^* = 1.19$ cm/s; (e) $\bar{h} = 0.55$ cm, $v^* = 1.37$ cm/s.

much faster as the frequency increases. This is evidently the result of the linear decay rates for waves of various frequencies which are proportional to liquid viscosity.

Next, the experimental data are compared to the predictions of [23]. The worst agreement between the experimental and theoretical results is seen in figure 7. In this figure, the liquid Reynolds number (R_L) is 255 based on the average layer depth and velocity; the wave field is two-dimensional until the gas Reynolds number (R_G) reaches ~ 7500. It appears that the spectral equation is slightly deficient when predicting the spectra of relatively sedate flow conditions. Although the results in figure 7 are not as quantitatively accurate as desired, the correct qualitative trends are present as the magnitude of ϕ increases and the peak shifts to higher frequencies with increasing friction velocity. However, the theoretical and experimental results coincide extremely well in figures 8–10 where the flow conditions create a rougher interface and an earlier R_G transition from a two-dimensional to a pebbly three-dimensional surface. In figure 11, which contains data for the largest R_L examined, the agreement is acceptable but a transition from over-predicting to under-predicting the magnitude of ϕ has begun—especially at the higher R_G values. We note that for the higher R_L and R_G values in these figures, a low frequency wave peak, which is not predicted by [2] is beginning to appear. Bruno & McCready (1988) have shown that this peak results from a growing linear instability of very-long-wavelength wave disturbances. The low frequency peaks would be even more prounced if better resolution at low frequencies were possible [see Bruno & McCready (1988) for example spectra]. However, this could be obtained only by digitizing the signal at a slower rate which would prevent resolution of the highest frequencies of interest.

At the flow conditions listed in figure 12, the interface is predominantly two-dimensional. As in figure 7 for water, the spectral equation's quantitative predictions for $\phi(f)$ are inaccurate (however generally within the correct order of magnitude), but the qualitative trends are correct. In figures 13 and 14 where the flow conditions are less tranquil, the experimental data are once again predicted moderately well. The results from the largest R_L at which data were taken are seen in figure 15. For these flow conditions the spectral equation also underestimates the magnitude $\phi(f)$ in the peak region. However, note that the theory has predicted the frequency spectra to be pinched

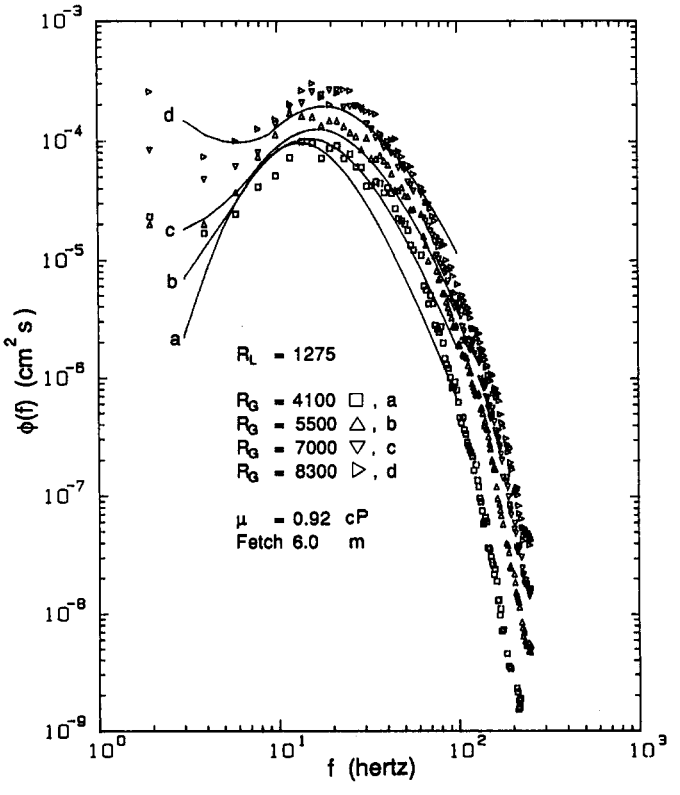

Figure 11. Comparison of experimental and theoretical wave spectra. (a) $\bar{h} = 0.84$ cm, $v^* = 0.71$ cm/s; (b) $\bar{h} = 0.81$ cm, $v^* = 0.88$ cm/s; (c) $\bar{h} = 0.74$ cm, $v^* = 1.00$ cm/s; (d) $\bar{h} = 0.66$ cm, $v^* = 1.21$ cm/s.

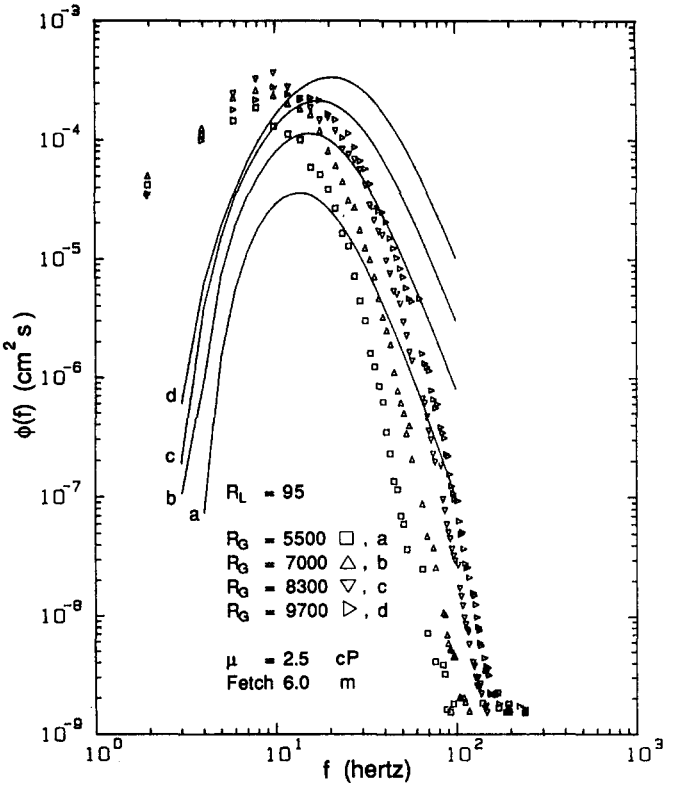

Figure 12. Comparison of experimental and theoretical wave spectra. (a) $\bar{h} = 0.38$ cm, $v^* = 0.76$ cm/s; (b) $\bar{h} = 0.35$ cm, $v^* = 0.91$ cm/s; (c) $\bar{h} = 0.33$ cm, $v^* = 1.09$ cm/s; (d) $\bar{h} = 0.30$ cm, $v^* = 1.20$ cm/s.

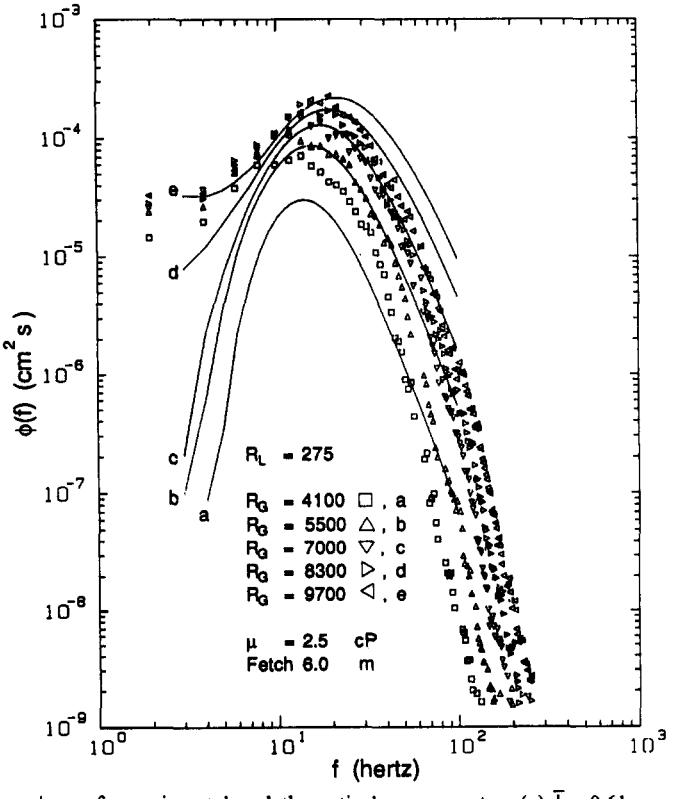

Figure 13. Comparison of experimental and theoretical wave spectra. (a) $\bar{h} = 0.61$ cm, $v^* = 0.68$ cm/s; (b) $\bar{h} = 0.60$ cm, $v^* = 0.88$ cm/s; (c) $\bar{h} = 0.58$ cm, $v^* = 1.04$ cm/s; (d) $\bar{h} = 0.54$ cm, $v^* = 1.25$ cm/s; (e) $\bar{h} = 0.51$ cm, $v^* = 1.38$ cm/s.

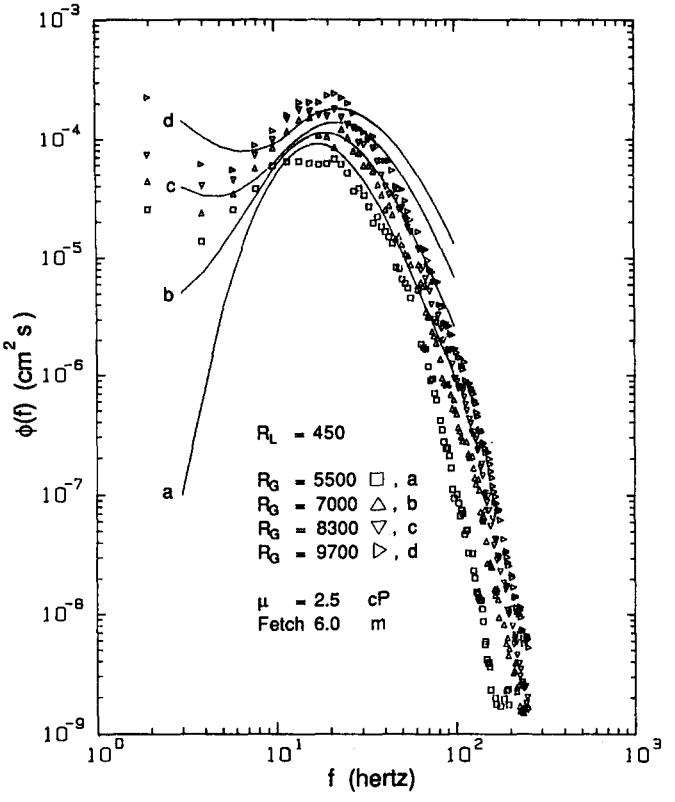

Figure 14. Comparison of experimental and theoretical wave spectra. (a) $\bar{h} = 0.71$ cm, $v^* = 0.94$ cm/s; (b) $\bar{h} = 0.69$ cm, $v^* = 1.16$ cm/s; (c) $\bar{h} = 0.65$ cm, $v^* = 1.32$ cm/s; (d) $\bar{h} = 0.61$ cm, $v^* = 1.63$ cm/s.

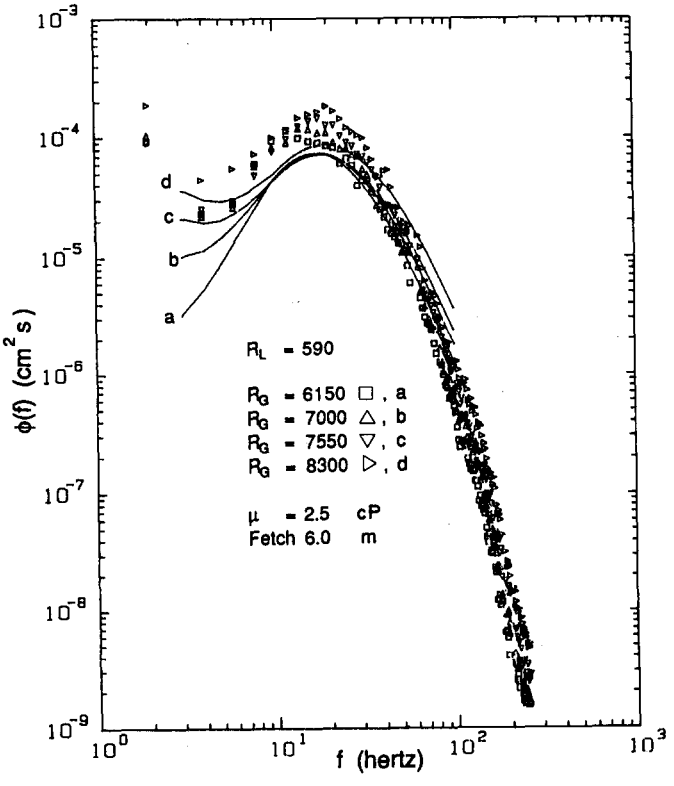

Figure 15. Comparison of experimental and theoretical wave spectra. (a) $\bar{h} = 0.86$ cm, $v^* = 1.10$ cm/s; (b) $\bar{h} = 0.86$ cm, $v^* = 1.21$ cm/s; (c) $\bar{h} = 0.87$ cm, $v^* = 1.29$ cm/s; (d) $\bar{h} = 0.80$ cm, $v^* = 1.36$ cm/s.

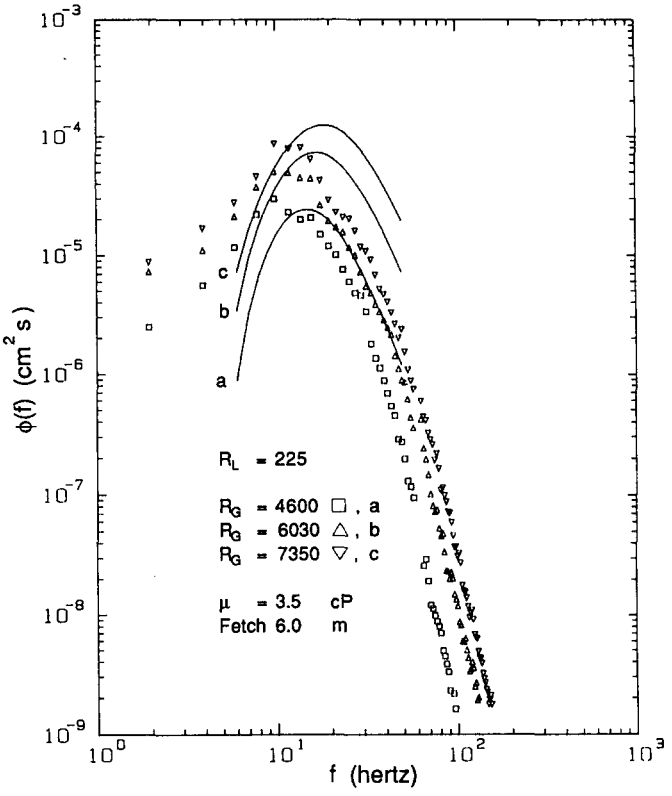

Figure 16. Comparison of experimental and theoretical wave spectra. (a) $\bar{h} = 0.56$ cm, $v^* = 0.70$ cm/s; (b) $\bar{h} = 0.53$ cm, $v^* = 0.90$ cm/s; (c) $\bar{h} = 0.52$ cm, $v^* = 1.05$ cm/s.

closely together, which is in qualitative agreement with the experimental spectra. This pinching is due to the influence of the layer depth and gas shear on the interaction time τ_I.

Figure 16 is included to demonstrate that expressing the geometric factor Q in terms of the viscosity ratio, is applicable to more than the two viscosities in figures 7–15. Because it is a constant, Q does not affect the shape of the spectrum, only its magnitude. Therefore, although the theoretical spectra in figure 16 are shifted too far to the right, defining Q as the ratio of viscosities appears to select the proper magnitude of $\phi(f)$.

Data were not taken at $R_L > 1275$ and $R_G > 9700$ for water and $R_L > 590$ and $R_G > 9700$ for 2.5 cP glycerin-water solutions because roll waves began to appear on the interface. These disturbances influence the shape of the spectrum and cannot be predicted by the spectral equation.

6. DISCUSSION

Ideally, one would like to predict the wave spectrum for arbitrary conditions and flow configurations. To do this, it is essential that all of the individual processes which control wave behavior be understood. The data shown in section 3 demonstrate rather dramatically that energy transfer between various modes exerts a strong role in determining the shape of the spectrum. It is interesting to note that the time scales for the rate of energy transfer, which are on the order of 1 s, shown in figures 1–4 for cases which do not satisfy resonant conditions, are similar or somewhat faster than those calculated by van Gastel (1987) for strongly resonant interactions. This indicates that significant energy transfer occurs between nonresonant waves at rates which are similar to the resonance case. Although the results of Kim & Hanratty (1971) and Janssen (1987) indicate that monotonic energy transfer can occur for a purely resonant case and that oscillatory transfer (which is less efficient) will occur for nearly-resonant interactions, the presence of dissipation which increases with frequency (and prevents some of the energy transferred upward

from returning downward) makes it necessary to consider all significant overtone interactions. Therefore, any theoretical description of the wave spectrum should not be limited to purely resonant interactions.

Our attempts to quantitatively predict the spectrum confirm the importance of interactions in determining the spectral shape. We found that it was essential to include the effects of shear and layer depth in the expression for the interaction rate otherwise discrepancies of an order of magnitude or more occurred when the results were compared to experimental data. For example, in figure 8, the range of theoretical peak spectral values would be two orders of magnitude instead of the actual one-half order of magnitude spread if the effects of depth and gas shear were not included. It also appears that fluids with different viscosities cause an additional complication because waves become more two-dimensional as the viscosity is increased. Spectra for the 2.5 cP liquid have peaks which are comparable to those for water at similar R_L and R_G values. However, the calculated growth rates are significantly higher for the 2.5 cP fluid because the layers are thicker suggesting that the spectral peaks should be larger as well. As the liquid velocity gradient is actually lower for the more viscous liquid and the layer is thicker (precluding an increase in the interaction rate because of shear or a lower layer depth), the only obvious physical explanation for the behavior is that interaction rates are faster because the waves are more two-dimensional. This is consistent with McGoldrick's (1965) theory for strong resonanace which also predicts a smaller time constant τ_1 for collinear wave fields. The need to use the first power (as opposed to a smaller power) of the visocity ratio in the expression for the interaction rate to match the data, demonstrates how significant effect this effect is.

Another issue is the prediction of the rate of energy input for the waves. Linear theories are probably justified because the wave slopes are observed to be small, however the question of how to deal with the turbulent gas flow remains. Two straightforward and computationally accessible approaches are available. One is to solve an Orr-Sommerfeld equation for the gas phase as well as the liquid, assuming appropriate velocity profiles and laminar flow. This approach has been used by several researchers including Benjamin (1959), Miles (1959), Kawai (1979) and van Gastel *et al.* (1985). The alternative is to include the effects of turbulence by using the measurements and calculations of Abrams (1984) (he has solved an Orr-Sommerfeld equation including a turbulence model). A comparison of these two approaches is shown in figures 17a and 17b. In figure 17a, theoretical values for $\hat{P}_{sl}$ (which dominates the growth process for a wide range of wavelengths), taken from the early work of Benjamin (1959) and the recent study of van Gastel *et al.* (1985), are compared to those measured and correlated by Abrams (1984). Several interesting features are noted. First, the two solutions of Benjamin, solid wall and mobile interface, are very similar in magnitude and shape, indicating that the different boundary conditions make little difference in the solution (this is expected because the viscosity ratio, μ_G/μ_L is very small). van Gastel's solution differs from Benjamin's primarily because a different average velocity profile is assumed for the gas and liquid phases. However, the effect of turbulence is substantial. Abrams' results indicate that turbulence causes a qualitative change in the behavior for small wavenumbers. For higher wavenumbers, the shape is the same with a small but significant quantitative difference occurring. In figure 17b, growth rates from various models are shown. It is seen that the shapes are similar, while the peak from Abrams' data is sharper and approximately twice as large. It is noted that while Kawai (1979) showed good agreement between measured growth rates and his theory, Janssen (1987) states that because the effect of nonlinear interactions between waves was neglected (when data are compared to theory), Kawai's theoretical growth rates may be as much as a factor of two too small. Therefore, one can at least tentatively conclude that because turbulence effects are so important, the use of relations developed from measured values for flow over solid wavy surfaces is appropriate for gas–liquid flows.

It is of interest to discuss the potential applicability of the present procedure for predicting the spectrum in other flow situations. Two cases important from a practical standpoint are annular and stratified flows in pipes. As mentioned above, if the layer thickness is much less than the wavelength of the dominant waves, such as occurs in annular flows where shear rates are exceedingly high, wave interactions do not occur and the wave spectrum is not governed by the dynamic process which was modeled here. However, for horizontal (or nearly horizontal) stratified flows, the wave spectrum will be determined by the same processes but with additional factors. The

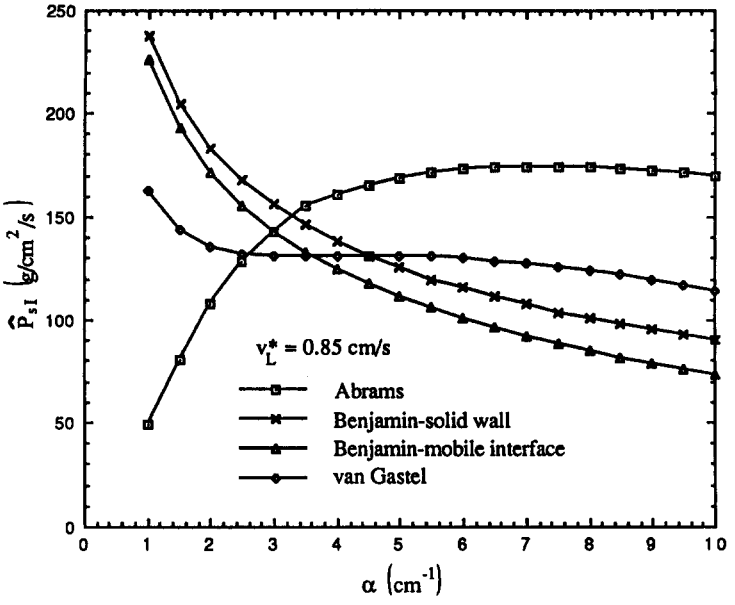

Figure 17a. Comparison of the magnitude of the pressure fluctuation component in phase with the wave slope as a function of wavenumber.

obvious complications which arise are those caused by the curvature of the pipe. Namely, the gas flow will have secondary currents which could cause some small changes in the energy input rate. In addition, the layer depth will not be constant. These effects can be expected to exert some minor quantitative changes in the spectrum. The present analysis would probably work well using an average depth. A potentially major change in the spectrum of capillary–gravity waves would occur if a significant gravity wave peak appears which would be possible in large (dia $\gtrsim$ 20 cm) conduits where liquid depths are $\gtrsim$ 10 cm. As noted by Bruno & McCready (1987), spectra (see Liu & Lin 1982) measured on deeper layers invariably have much larger magnitude spectral values for the 10–100 Hz range than those measured in a small channel. The probable explanation for this is the

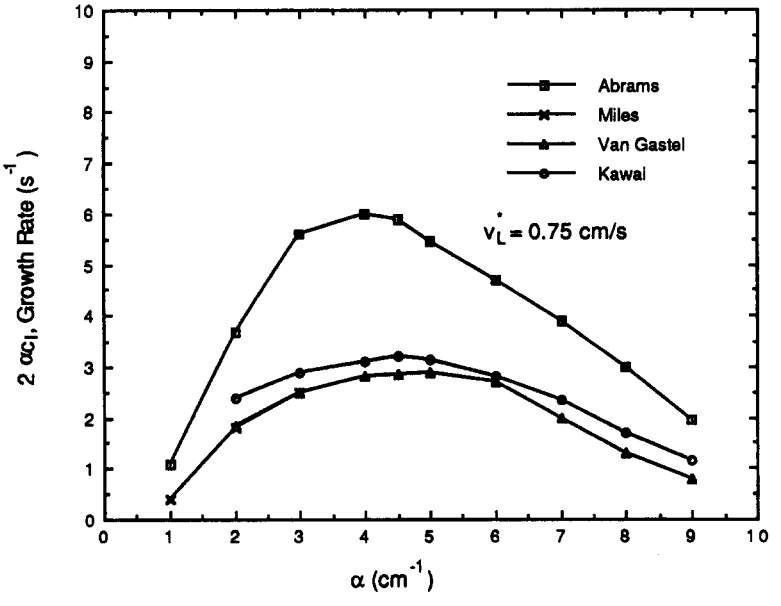

Figure 17b. Comparison of theoretical wave growth rates as a function of wavenumber to the growth rate calculated using the empirical correlation of Abrams (1984).

instability of the peaks of gravity waves in the presence of surface tension which causes parasitic capillary waves to form in front of the gravity wave peak. Those parasitic waves can contribute substantially to the magnitude of the spectrum because their parent gravity waves provide an essentially infinite (relative to the capillary wave) energy source. Quantitative descriptions of this effect for regular periodic waves have been given by Longuet-Higgins (1963) and Crapper (1970). Measurements by Chang *et al.* (1978) clearly show the appearance and magnitude of these waves. The theory described above does not account for this direct type of energy transfer from gravity waves to much smaller capillary waves. As a consequence, wave spectra in stratified flows where the liquid is deep could be expected to have high frequency wave spectra which are substantially higher than those predicted by [23].

Acknowledgements—This work is being supported by the Department of Energy under Grant DEFG02-88ER13913.

REFERENCES

ABRAMS, J. 1984 Turbulent flow over small amplitude solid waves. Ph.D. Thesis, Univ. of Illinois, Urbana.

ANDREUSSI, P., ASALI, J. C. & HANRATTY, T. J. 1985 Initiation of roll waves in gas–liquid flows. *AIChE Jl* **31,** 119–126.

ANDRITSOS, N. & HANRATTY, T. J. 1987 Influence of interfacial waves in stratified gas–liquid flows. *AIChE Jl* **33,** 444–454.

BACK, D. D. & MCCREADY, M. J. 1988a Effect of small wavelength waves on gas transfer across the ocean surface. *J. geophys. Res.* **93,** 5143–5152.

BACK, D. D. & MCCREADY, M. J. 1988b Theoretical study of interfacial mass transport in gas–liquid flows. *AIChE Jl* **34,** 1789–1802.

BENJAMIN, T. B. 1959 Shearing flow over a wavy boundary. *J. Fluid Mech.* **6,** 161–205.

BRUNO, K. 1988 The study of interfacial waves in gas–liquid flows. Ph. D. Thesis, Univ. of Notre Dame, Ind.

BRUNO, K. & MCCREADY, M. J. 1987 Theoretical considerations in the prediction of wave behavior in gas–liquid flows. Presented at the *AIChE A. Mtg*, New York, Paper 79F.

BRUNO, K. & MCCREADY, M. J. 1988 Origin of roll waves in gas–liquid flows. *AIChE Jl* **34,** 1431–1440.

CHANG, J. H., WAGNER, R. N. & YUEN, H. C. 1978 Measurement of high frequency capillary waves on steep gravity waves. *J. Fluid Mech.* **86,** 401–413.

COHEN, L. S. 1964 Interaction between turbulent air flow and a flowing liquid film. Ph. D. Thesis in Chemical Engineering, Univ. of Illinois, Urbana.

COHEN, L. S. & HANRATTY, T. J. 1965 Generation of waves in the concurrent flow of air and a liquid. *AIChE Jl* **11,** 138–144.

CRAPPER, G. D. 1970 Non-linear capillary waves generated by steep gravity waves. *J. Fluid Mech.* **40,** 149–159.

VAN GASTEL, K. 1987 Nonlinear interactions of gravity–capillary waves: Lagrangian theory and effects on the spectrum. *J. Fluid Mech.* **182,** 499–523.

VAN GASTEL, K. JANSSEN, P. A. E. M. & KOMEN, G. J. 1985 On phase velocity and growth rate of wind-induced gravity–capillary waves. *J. Fluid Mech.* **161,** 199–216.

HANRATTY, T. J., 1983 Interfacial instabilities caused by air flow. In *Waves on Fluid Interfaces* (Edited by MEYER, R. E.). Academic Press, New York.

HANRATTY, T. J. & ENGEN, J. M. 1957 Interaction between a turbulent air stream and a moving water surface. *AIChE Jl* **3,** 299–304.

HASSELMANN, K., 1962 On the non-linear energy transfer in a gravity wave spectrum. Part 1. *J. Fluid Mech.* **12,** 481–500.

HASSELMANN, K., 1963 On the non-linear energy transfer in a gravity wave spectrum. Part 2. *J. Fluid Mech.* **15,** 273–281.

HEISENBERG, W. 1948 Zur statistischen Theorie der Turbulenz. *Z. Phys.* **124,** 628–635.

HICKS, B. L., 1960 The energy spectrum of small wind waves. Univ. Illinois C.S.L. Report No. M-92.

JANSSEN, P. A. E. M. 1986 The period-doubling of gravity–capillary waves. *J. Fluid Mech.* **172,** 531–546.

JANSSEN, P. A. E. M. 1987 The initial evolution of gravity–capillary waves. *J. Fluid Mech.* **184,** 581–597.

KAWAI, S. 1979 Generation of initial wavelets by instability of a coupled shear flow and their evolution of wind waves. *J. Fluid Mech.* **93,** 661–703.

KIM, Y. Y. & HANRATTY, T. J. 1971 Weak quadratic interactions of two-dimensional waves. *J. Fluid Mech.* **50,** 107–132.

LARSON, T. R. & WRIGHT, J. W. 1975 Wind-generated gravity–capillary waves: laboratory measurements of temporal growth rates using microwave backscatter. *J. Fluid Mech.* **70,** 417–436.

LILLELEHT, L. U. & HANRATTY, T. J. 1961 Relation of interfacial shear stress to the wave height for concurrent air–water flow *AIChE Jl* **7,** 548–550.

LIN, P. Y. & HANRATTY, T. J. 1986 Prediction of the initiation of slugs with linear stability theory. *Int. J. Multiphase Flow* **12,** 79–98.

LIU, H.-T. & LIN, J.-T. 1982 On the spectra of high-frequency wind waves. *J. Fluid Mech.* **123,** 165.

LLEONART, G. T. & BLACKMAN, D. R. 1980 The spectral characterisics of wind-generated capillary waves. *J. Fluid Mech.* **97,** 455–479.

LONGUET-HIGGINS, M. S. 1963 The generation of capillary waves by steep gravity waves. *J. Fluid Mech.* **16,** 138–159.

MCCREADY, M. J. 1986 Spectral behavior of capillary waves in gas–liquid flows. *Phys. Fluids* **29,** 2836–2842.

MCCREADY, M. J. & HANRATTY, T. J. 1985 Effect of air shear on gas absorption by a liquid film. *AIChE Jl* **31,** 2066–2074.

MCGOLDRICK, L. F. 1965 Resonant interactions among capillary–gravity waves. *J. Fluid Mech.* **21,** 305–301.

MILES, J. W. 1959 On the generation of surface waves by turbulent shear flows. Part 2. *J. Fluid Mech.* **6,** 568–582.

MIYA, M., WOODMANSEE, D. E. & HANRATTY, T. J. 1971 A model for roll waves in gas–liquid flows. *Chem. Engng Sci.* **26,** 1915–1923.

PAO, Y.-H. 1965 Structure of turbulent velocity and scalar fields at large wavenumbers. *Phys. Fluids* **8,** 1063–1075.

PHILLIPS, O. M. 1958 The equilibrium range in the spectrum of wind-generated waves. *J. Fluid Mech.* **4,** 426–434.

PHILLIPS, O. M. 1985 Spectral and statistical properties of the equilibrium range in wind-generated gravity waves. *J. Fluid Mech.* **156,** 505–531.

TAITEL Y. & DUKLER, A. E. 1976 A model for predicting flow regime transitions in horizontal and near horizontal gas–liquid flow. *AIChE Jl* **22,** 47–55.

TELLES, A. S. & DUKLER, A. E. 1970 Statistical characteristics of thin, vertical, wavy, liquid films. *Ind. Engng Chem. Fundam.* **9,** 412–421.

VALENZUELA, G. R. & LAING, M. B. 1972 Nonlinear energy transfer in gravity–capillary wave spectra, with applications. *J. Fluid Mech.* **54,** 507–520.

WEBB, D. R. & HEWITT, G. F. 1975 Downwards co-current annular flow. *Int. J. Multiphase Flow* **2,** 35–49.

WOODMANSEE, D. E. and HANRATTY, T. J. 1979 Mechanism for removal of droplets from a liquid surface by a parallel air flow. *Chem. Engng Sci.* **24,** 299–307.